Supplementary Information for: Simulating Open Quantum Systems with Molecular Spin Qudits

Sebastián Roca-Jerat,[1,2] Emilio Macaluso,[3] Alessandro Chiesa,[3,4,5] Paolo Santini,[3,4,5] and Stefano Carretta[3,4,5,*]

[1] *Instituto de Nanociencia y Materiales de Aragón (INMA), CSIC-Universidad de Zaragoza, Zaragoza 50009, Spain*
[2] *Departamento de Física de la Materia Condensada, Universidad de Zaragoza, Zaragoza 50009, Spain*
[3] *Universitá di Parma, Dipartimento di Scienze Matematiche, Fisiche e Informatiche, 43124 Parma, Italy*
[4] *UdR Parma, INSTM, I-43124 Parma, Italy*
[5] *Gruppo Collegato di Parma, INFN-Sezione Milano-Bicocca, I-43124 Parma, Italy*

I. ON THE NUMERICAL SIMULATIONS

All numerical simulations presented in the main text have been carried out by integrating the Lindblad equation for the complete system, which comprises both the molecular complexes (described by the spin operators $S_{\alpha,i}$, with $\alpha = x, y, z$ and $i = 1, \dots n$) and the superconducting resonator (described by the creation/annihilation operators $a^\dagger/a$). Being H the Hamiltonian that describes the interaction between all components and fixes the level spectrum (Eq. (4) in the main text) and ρ the density matrix for the whole system, this equation reads

$$\begin{aligned} \dot{\rho} &= -i[H + H_1(t), \rho] \\ &+ \frac{1}{T_2} \sum_i \left(2S_{zi}\rho S_{zi} - S_{zi}^2\rho - \rho S_{zi}^2\right) \\ &+ \frac{\omega_r}{2\pi Q} \left(2a\rho a^\dagger - a^\dagger a\rho - \rho a^\dagger a\right) \ . \end{aligned} \tag{1}$$

As can be seen, we include in the simulations the most relevant dissipation phenomena in our implementation: decoherence (T_2) and photon loss ($\omega_r/2\pi Q$). The coherent dynamics generated by the different microwave pulses is encapsulated in the $H_1(t)$ term. All the simulations have been conducted on the interaction picture and the driving pulses have been parameterized as Gaussian pulses with a maximum amplitude of 60 G. On the other hand, to alleviate the computational cost of the simulations, it has been chosen to consider zero leakage during the coherent evolution induced by the microwave pulses. That is, it is assumed that for a pulse with frequency ω, only population transfer occurs between those states $|i\rangle, |j\rangle$ where $\omega = \omega_{ij}$, being ω_{ij} the energy difference between those states. The exact diagonalization to obtain the spectra of the different compounds, as well as the eigenstates, has been carried out using *Numpy*[1] while for the integration of the dynamics we have used *Qutip*[2], all *Python* libraries.

II. ALGORITHM IN WHICH THE ANCILLA MIMICS THE ENVIRONMENT

A. On the algorithm & the hardware

As described in the main text, to implement this algorithm we need two registers[3]. One of them acts as the system of interest (1/2-spin) while the other acts as the environment (DEP channel). The dynamics we want to convert into a quantum circuit are described by a set of Kraus operators, $\{E_k\}$, such that

$$\mathcal{E}(\rho_{\text{in}}) = \sum_k E_k \rho_{\text{in}} E_k^\dagger = \rho_{\text{out}} \ . \tag{2}$$

The first step to implement this dynamic consists of expressing the set of Kraus operators as a linear combination of unitary operators, $E_k = \sum_{i=0}^{d-1} c_k^i U_i$ with c_k^i real coefficients and $\{U_i\}$ the set of unitaries. The dimension of this set $\{U_i\}$ determines the dimension of the ancilla system that acts as the environment. Moreover, these unitaries correspond to the controlled unitaries that appear in the circuit of Figure 1b of the main text and that reflect the type of interaction between system of interest and environment. The coefficients c_k^i store the intensity of such interaction and fix the first column of the operator V. The remaining columns of this matrix V can be arbitrarily filled with orthonormal vectors. Note that since the ancilla must always start in its ground state, the amplitudes of its wave function after applying V are determined only by this first column. Finally, the operation W is determined through the relation $E_k = \sum_{i=0}^{d-1} W_{ki} V_{i0} U_i$. For convenience, recall that in our case we work with the DEP channel, which is described by the set of Kraus operators $\{E_k\}_{k=0}^3 = \left\{\sqrt{1-\frac{3p}{4}}\mathcal{I}, \sqrt{\frac{p}{4}}\sigma_x, \sqrt{\frac{p}{4}}\sigma_y, \sqrt{\frac{p}{4}}\sigma_z\right\}$, which can be directly related to the unitaries $\{U_k\}_{k=0}^3 = \{\mathcal{I}, \sigma_x, \sigma_y, \sigma_z\}$ with the coefficients $\{c_k\}_{k=0}^3 = \left\{\sqrt{1-\frac{3p}{4}}, \sqrt{\frac{p}{4}}, \sqrt{\frac{p}{4}}, \sqrt{\frac{p}{4}}\right\}$. The matrices V and W therefore have the following expressions

$$V = \begin{pmatrix} \sqrt{1-\frac{3p}{4}} & -\sqrt{\frac{\frac{p}{4}(1-\frac{3p}{4})}{1-\frac{p}{4}}} & -\sqrt{\frac{\frac{p}{4}(1-\frac{3p}{4})}{(1-\frac{p}{4})(1-\frac{p}{2})}} & -\sqrt{\frac{p}{4-2p}} \\ \sqrt{\frac{p}{4}} & \sqrt{1-\frac{p}{4}} & 0 & 0 \\ \sqrt{\frac{p}{4}} & -\frac{p}{4\sqrt{1-\frac{p}{4}}} & \sqrt{\frac{1-\frac{p}{2}}{1-\frac{p}{2}}} & 0 \\ \sqrt{\frac{p}{4}} & -\frac{p}{4\sqrt{1-\frac{p}{4}}} & -\frac{p}{4\sqrt{(1-\frac{p}{4})(1-\frac{p}{2})}} & \sqrt{\frac{4-3p}{4-2p}} \end{pmatrix} \text{ and } W = \mathcal{I} = \begin{pmatrix} 1 & 0 & 0 & 0 \\ 0 & 1 & 0 & 0 \\ 0 & 0 & 1 & 0 \\ 0 & 0 & 0 & 1 \end{pmatrix} \ .$$

The parameter p describes the intensity of the depolarizing channel but has no time dependence. To express this parameter as a function of a characteristic time, T_{DEP}, we can relate the dynamics generated by the Kraus based dynamic map to the equivalent dynamics described by the master equation $\dot{\rho}(t) = \sum_{\alpha=x,y,z} \left[\sigma_\alpha \rho \sigma_\alpha^\dagger - \frac{1}{2}\left\{\sigma_\alpha^\dagger \sigma_\alpha, \rho\right\}\right]$. By tracing the equivalence in the dynamics of the matrix elements of ρ we get that $p = 1 - e^{4t/T_{DEP}}$.

Since we need a two-level system to act as the spin 1/2 of interest and an ancilla with 4 levels to act as the DEP channel, we choose the molecular complex proposed in Ref. 4 modified to accommodate a 3/2-spin (unit B) coupled to the 1/2-spin (unit A) through the dimer (M_{AB}) [Cf. Figure 2a in the main text]. The presence of the dimer as a switch for the interactions between the two units is very convenient for this algorithm. The parameters chosen for the spin Hamiltonian describing the system

$$H_{AMB}^{(M1)} = \mu_B B_0 \left(g_z^A S_z^A + g_z^B S_z^B + g_z^M \left(S_{1z}^M + S_{2z}^M\right)\right) + D_B \left(S_z^B\right)^2 + \Delta \mathbf{S}_1^M \cdot \mathbf{S}_2^M + J \sum_{\alpha=A,B} \sum_{i=1,2} \mathbf{S}_\alpha \cdot \mathbf{S}_i^M \,, \qquad (3)$$

are $g_z^A = 1.84$, $g_z^B = 1.98$, $g_z^1 = g_z^2 \equiv g_z^M = 2.1$, $\Delta/2\pi = 30$ GHz, $J/2\pi = 0.2$ GHz, $D_B/2\pi = 5.2$ GHz, $B_0 = 700$ mT. Several comments are relevant here. First, note that although the choice of these parameters has been based on typical values present in the literature for different compounds, the validity of the algorithms is independent of these. Second, in this particular implementation it is especially important that the interaction between the spins within the dimer is sufficiently stronger than the interaction between the dimer and the other units, $\Delta \gg J$, so that the wave function of the system is sufficiently factorized to consider each unit as independent in practice. On the other hand, for us to be able to make transitions between the singlet and triplet of the dimer, it is necessary that there is a difference in the gyromagnetic factors of the dimer spins in the direction in which the magnetic field that generates the control pulses is applied. In our case, we consider that the two Cu^{2+} ions forming the dimer are rotated about their axis such that $g_x^1 - g_x^2 = 0.2$, $g_y^2 - g_y^1 = 0.2$ and $g_z^1 = g_z^2 = 2.1$. For the other units we simply choose $g_x^{A,B} = g_z^{A,B}$. Finally, the DC magnetic field, B_0, is applied in the Z direction for simplicity in order to identify the system states as the logical levels on which to perform the computation. This combination of parameters gives rise to the resonance frequencies of both the transitions that take place in the logical subspace (transitions that only affect unit A or unit B) and the auxiliary transitions that serve us for both units to interact (excitations from the singlet to the dimer triplet) presented in Figure S1. As we can see, we have four transitions in the logical space corresponding to the only possible transition of spin 1/2 (A) and the 3 transitions of the 4-level system (B). All degeneracies correspond to excitations of one of the units while the other remains at the same state.

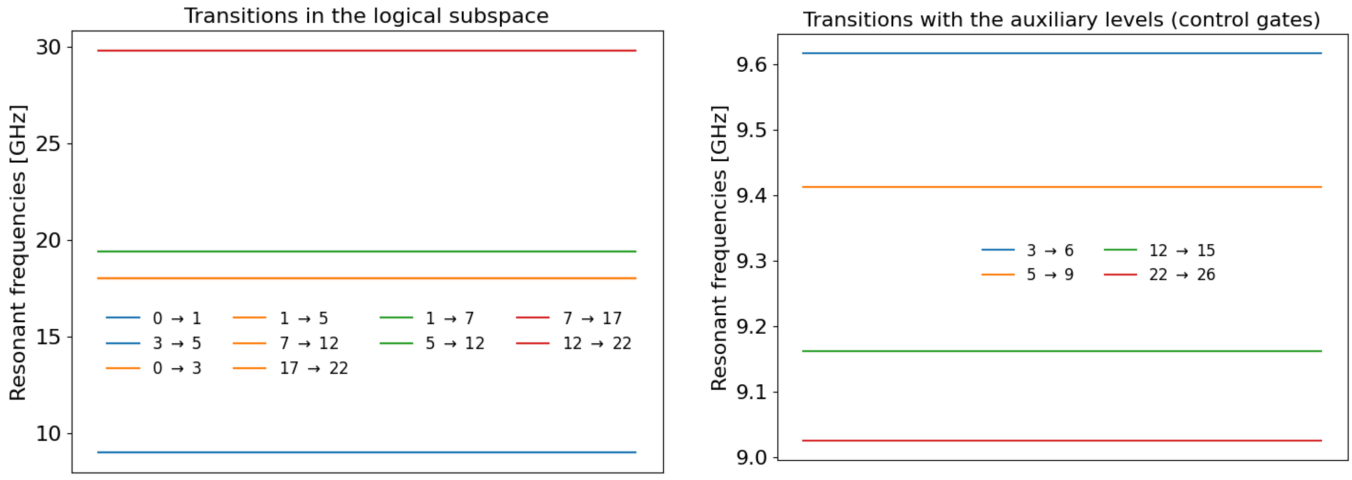

FIG. S1. Resonant frequencies for the different transitions addressed in the single qubit simulation.

Although we do not consider the leakage effects that occur when two frequencies are too close to each other, we consider that the separation between levels should not be problematic. Moreover, with the chosen parameters we achieve that all frequencies are below the 30 GHz threshold, which is convenient for microwave electronics. To be more specific about the type of transitions that take place, in the logical subspace the transitions take place between levels $|-1/2, m_B, S\rangle$ and $|+1/2, m_B, S\rangle$ for unit A and between $|m_A, m_B, S\rangle$ and $|m_A, m_B \pm 1, S\rangle$ for unit B, where S stands for the singlet state of the dimer. In the case of the auxiliary transitions, the four transitions correspond to exciting the singlet dimer to one of the triplet states for each of the qudit states while the qubit A is in the $+1/2$ state, $|+1/2, m_B, S\rangle \rightarrow |+1/2, m_B, T\rangle$. As demonstrated in Ref. 4, these auxiliary transitions allow us to perform Cφ

operations that generate entanglement between units A and B. To achieve a Cφ gate on A conditioned on the state of B we only need to perform two consecutive π pulses with a phase difference of φ between them. If the phase difference is zero, we implement a CZ gate between the qubit A and the qudit B. This, combined with single qubit gates on A allow us to implement all the controlled operations necessary to obtain the DEP channel dynamics: CX, CY and CZ. The microwave pulses applied on the transitions of the logic subspace give rise to planar rotations between the levels involved, the combination of which gives rise to any unitary gate we desire[5,6]. Thus, with all these ingredients we almost have what we need for the implementation of the circuit described in Figure 1b of the main text. The only thing we are missing is the mechanism to generate projective measures on the qudit, to trace out its degrees of freedom and thus acting non-coherently on the qubit.

To perform these projective measurements we make use of a superconducting resonator to which our molecular complex is coupled[6]. The coupling between these two systems is given by Eq. (4) of the main text and the value considered here is $G/2\pi = 100$ kHz. This value aligns with the estimates presented in Ref. 6. To perform these projective measurements, we follow the strategy detailed in Ref. 6. However, in our numerical simulations, since we have access to the full density matrix of the whole system, we do not perform the "experimental" measurement process, but directly perform the partial trace over the degrees of freedom of the qudit. Anyway, in order to include the effect that the decoherence could have on the system during this measurement process, after the application of all the pulses corresponding to all the gates of the circuit, we include a free evolution of duration equal to the estimated time in which this measurement would occur. To perform the projective measurement, the resonator frequency, ω_r, is set so that it is in resonance with the frequency of one of the transitions $|i\rangle \to |j\rangle$. If the state $|j\rangle$ is populated, a photon will be emitted which can be annihilated by a counter. Tunability in this kind of resonators can be achieved through SQUIDs, which allow a change in resonator frequency of up to 30% in times as fast as 1 ns[6–8]. After applying the circuit, the state of the qudit will be $|\psi_B\rangle = \sqrt{1-\frac{3p}{4}}|0\rangle + \sum_{j=1}^{3}\sqrt{\frac{p}{4}}|j\rangle$. The probability of emitting a photon is then $p/4$ if the system is in any of the $|j=1,2,3\rangle$ states. Note that, if the system is in the $|0\rangle$ state, no photon will be detected. Since we usually consider dynamics involving values of p small enough that the amplitude of $|0\rangle$ is the largest, it is convenient to encode this information in any other state to increase the probability of detecting a photon in less time. Ultimately, this encoding is completely arbitrary and simply changes the state of the qudit that conditions each of the controlled unitaries on the qubit. Therefore, if we choose for example the encoding such that the wave function is $|\psi_B\rangle = \sqrt{1-\frac{3p}{4}}|1\rangle + \sqrt{\frac{p}{4}}\left(|0\rangle + |2\rangle + |3\rangle\right)$, the average waiting time to observe a photon will be $\langle t_{\text{meas}}\rangle = \tau_{12}\left(1-3p/4\right) + (\tau_{01}+\tau_{12})p/4 + (\tau_{01}+\tau_{12}+\tau_{23})2p/4$, with τ_{ij} being the time it takes to complete half a Rabi cycle for the transition $i \to j$. In our case, $\tau_{01} = \tau_{23} = 1458$ ns and $\tau_{12} = 1263$ ns. In the simulations carried out to obtain the results shown in the different figures of the main text related to this method, the p parameter takes values approximately between 0.01 and 0.1, so that $\langle t_{\text{meas}}\rangle \approx 1.3$ μs.

B. On the complexity reduction

Once the hardware and the types of operations needed to implement the circuit imposed by the algorithm are established, we proceed to discuss the origin of the significant complexity reduction achieved by using qudits. As mentioned in the main text, the issue with qubit-based platforms relies in requiring numerous non-local gates, such as Toffoli. In Ref. 3, an estimation of the gate complexity scaling for this algorithm is developed as a function of the system size to be simulated. For a target system encoded in N qubits, and considering the most general case where $2N$ ancillary qubits are needed to simulate the bath (a scenario where the rank of the Kraus map is maximum), the gate complexity scales as $\mathcal{O}(8N^3 2^{4N} + N^2 2^{2N})$. In the case of qudits, let d_s be the dimension of the target system. Considering the same scenario as before, the dimension of the ancilla register will be up to d_s^2. We focus on the study of a system with spin $S \geq 1/2$ coupled to a Markovian bath, so that its extension to the case of a spin chain can be considered as a repetition of the single spin–single bath block. Thus, we need to decompose operations involving two qudits, one of dimension d_s and another of dimension d_s^2. Let's begin with the operations V and W that act on the ancilla. The first one is the simplest, as the register will always be initialized in the ground state, $|0\rangle$. Therefore, we only need to apply the first column of V, which corresponds to $d_s^2 - 1$ planar rotations[5,6]. For the more general operation W, we will need up to $\mathcal{O}(d_s^4)$ planar rotations. For the spin-bath interaction, we need to implement d_s^2 $C^m[U]$ controlled operations, where $m = 0, \ldots, d_s^2 - 1$ represents the subspace of the ancilla controlling the operation U. Following the decomposition proposed in Ref. 9, we need to implement 2 single-qudit gates on the target register and $d_s - 1$ CRz gates on the target, controlled by the state m of the ancilla. Additionally, there is a final operation on the ancilla to correct relative phases which could correspond to $d_s^2 - 1$ Rz gates. Thanks to the use of the dimer in our setup as a switch for the interactions between the spin and the bath, each of these CRz gates can be applied using two pulses of the same duration but with different phases[4]. This approach significantly alleviates the gate complexity of the implementation. Summing everything up, the total gate complexity for a single Trotter step of the incoherent

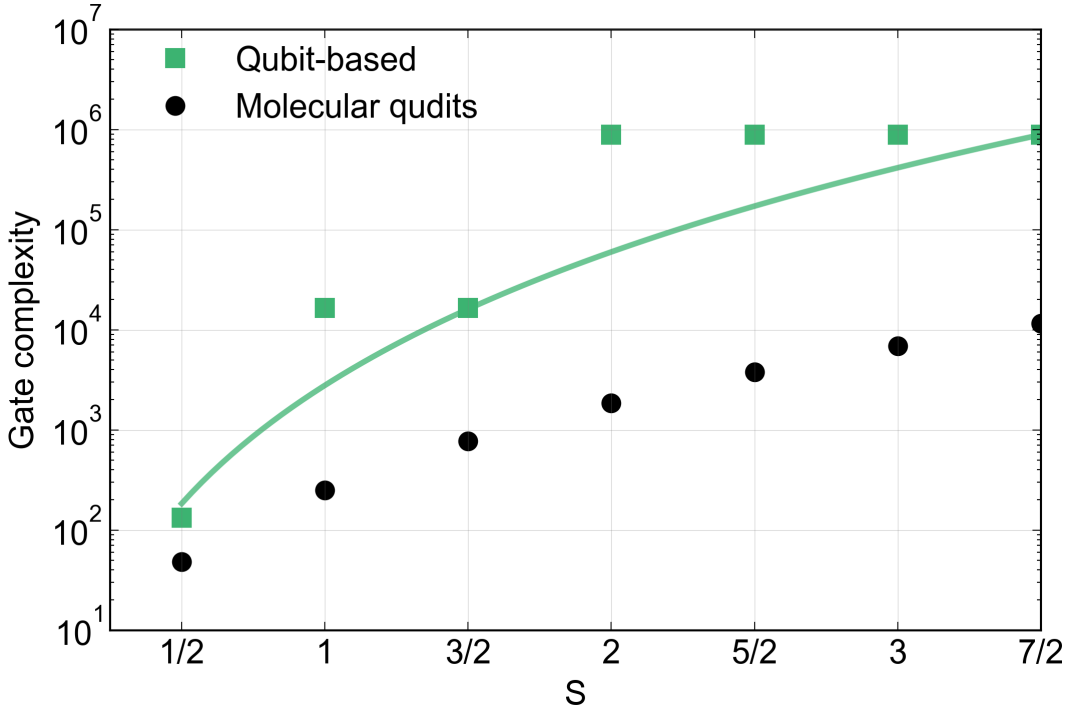

FIG. S2. Gate complexity scaling with the considered spin size S for each platform (qubit vs. qudit). The solid line shows the trend in gate complexity when considering dimensions that are powers of 2.

part of the dynamics is on the order of $\mathcal{O}(3d_s^4 + 4d_s^3 + d_s^2)$.

To make the comparison with qubits, we consider that to simulate a particle with spin S, we need $N = \lceil \log_2(2S+1) \rceil$ qubits. In Figure S2, we show the scaling behavior of each platform with respect to the spin considered. It is from this analysis that the values in the histogram shown in Figure 1b of the main text are derived. The plateaus that appear correspond to values of S that are not powers of 2. Here, the number of operations to be implemented is being overestimated because, although the number of required qubits remains the same, there are levels that are not utilized. The solid green line indicates the expected trend, obtained from a fit considering only the cases where $2S+1$ is a power of 2. The fact that not all the levels in the register are used highlights another inefficiency of using qubits in this context.

On the other hand, we are assuming that only one qudit is needed for each register, as there are proposals for molecules that could be used as qudits for the S values considered in the main text. In cases where more than one qudit would be necessary to accommodate all the degrees of freedom of the ancilla, for example, estimating the complexity becomes non-trivial. Nevertheless, the conclusions remain the same: reducing the number of units by using systems with more than two levels reduces the complexity of non-local operations and, therefore, the total gate complexity.

As a final remark, we find it important to highlight another common issue in typical NISQ devices, which is the connectivity between units (qubits). In the previous discussion, we did not account for the possibility of limited connectivity, which could necessitate certain SWAP operations. To provide a more concrete comparison, we utilize IBM's library, *Qiskit*[10], which allows us to obtain the decomposition of any circuit for a given architecture. Considering the case of a $1/2$ spin coupled to a 4-level bath, we require a circuit with 3 qubits. Figure S3 shows the circuit obtained by *Qiskit* where only single and two-body gates are present. The depth of this circuit is 64 gates. Note that here appear totally general gates. If we restrict the available gates to the typical native gates (SX, X, RZ and CNOT), the *Qiskit* decomposer, at its maximum optimization level, has given us 142 ± 4 gates after averaging over 50 instances. In this case the connectivity between qubits is the usual linear structure: $q_0 - q_1 - q_2$. In contrast, our implementation requires only 10 microwave pulses. To implement the V gate, since we only have to implement the first column as detailed above, only 3 planar rotations are necessary to initialize the 4 amplitudes of the qudit. Then, of the three controlled operations needed, two of them (the CX and CY gates) require two planar rotations on the qubit and a 2π pulse in the auxiliary subspace, while the CZ gate only requires a single 2π pulse in the auxiliary subspace.

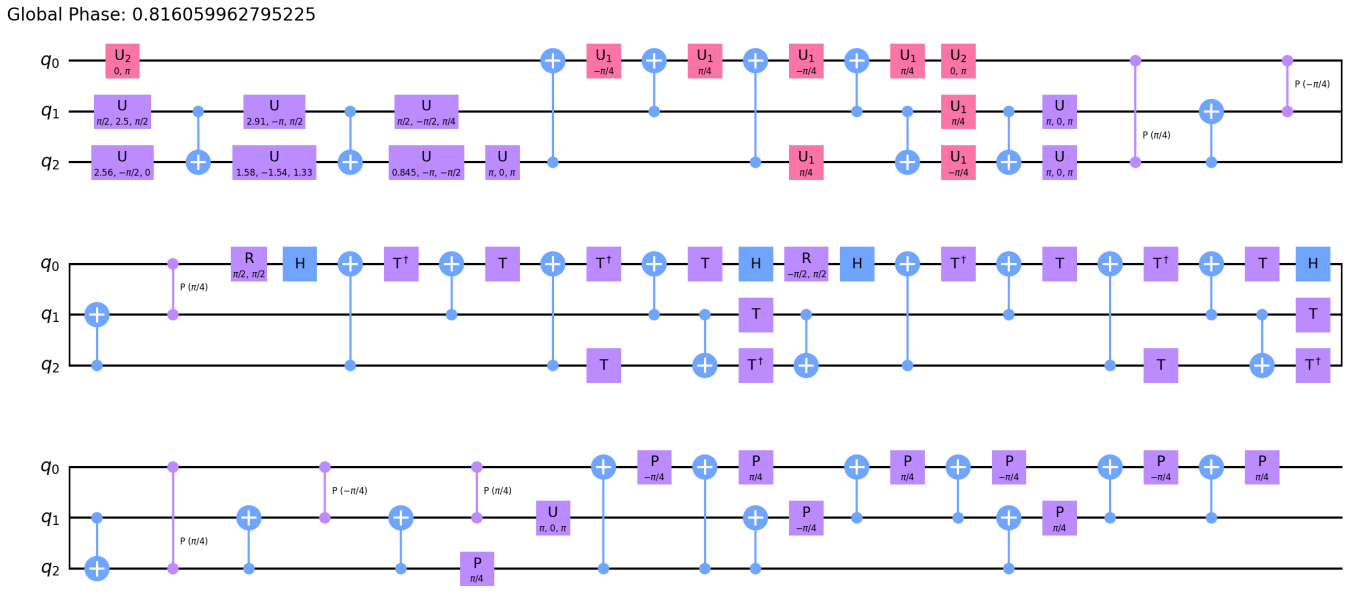

FIG. S3. Circuit decomposition for the DEP channel given by Qiskit until one only has one and two-body gates. The depth of this circuit is of 64 gates. To obtain this circuit, an arbitrary p value of $p = 0.01$ has been set.

III. ALGORITHM WITH FIXED ANCILLA DIMENSION

A. On the algorithm & the hardware

In this algorithm we work on the vectorized version of the density matrix. This means that, for a single two-level system or qubit, instead of considering a state by a density matrix $\rho = \begin{pmatrix} \rho_{00} & \rho_{01} \\ \rho_{10} & \rho_{11} \end{pmatrix}$, we now describe it by a vector $|\rho\rangle = \begin{pmatrix} \rho_{00} \\ \rho_{10} \\ \rho_{01} \\ \rho_{11} \end{pmatrix}$. As can be seen, this vector is constructed by stacking the columns of the previous matrix. Note that if we now want to encode this vector in a quantum circuit, we will need in principle 4 levels to store the corresponding coefficients. Thus, given a certain system of dimension d_s that is in a state $|\rho\rangle$, its time evolution will be given by the superoperator $\mathcal{L}$,

$$\mathcal{L} = -iI \otimes \mathcal{H} + i\mathcal{H}^T \otimes I + \sum_k \left(L_k^* \otimes L_k - \frac{1}{2} I \otimes L_k^\dagger L_k - \frac{1}{2} L_k^T L_k^* \otimes I \right) , \tag{4}$$

where I denotes the $d_s \times d_s$ identity operator, L_k are the Lindbladian operators describing the interaction between the system and the environment and the superscripts T, $*$ represent the transpose and the complex conjugate operators, respectively. At a certain instant t, the state of the system will be determined by solving the differential equation $\frac{d|\rho\rangle}{dt} = \mathcal{L}|\rho\rangle$. If $\mathcal{L}$ does not have an explicit time dependence, the integration can be performed and it follows that the evolution is determined by the operator $M = e^{\mathcal{L}t}$, $|\rho(t)\rangle = M|\rho(t_0)\rangle$. This operator M is the one we want to implement by means of a quantum circuit. Note that in this case it is not necessary to apply any Trotter-like decomposition since all the dynamics (coherent and incoherent) are included jointly in this operator. By applying the M operator we are able to go from any initial state to its corresponding final state in a single step. However, we still face the problem of implementing a non-unitary operator through unitary operators. Following the recipe given in Ref. 11, we can decompose this operator M into its hermitic and antihermitic parts, $M = S + A$. Here S corresponds to the hermitic part, $S = \frac{1}{2}(M + M^\dagger)$, while A corresponds to the antihermitic one, $A = \frac{1}{2}(M - M^\dagger)$. In turn, we can approximate these parts to a sum of operators that are unitary by means of

$$S = \lim_{\epsilon \to 0} \frac{i}{2\epsilon} \left(e^{-i\epsilon S} - e^{i\epsilon S} \right) = \lim_{\epsilon \to 0} \frac{1}{2\epsilon} \left(S_m - S_p \right) \tag{5}$$

and

$$A = \lim_{\epsilon\to 0} \frac{1}{2\epsilon}\left(e^{\epsilon A} - e^{-\epsilon A}\right) = \lim_{\epsilon\to 0} \frac{1}{2\epsilon}\left(A_p - A_m\right) \tag{6}$$

So that in the end

$$M = e^{\mathcal{L}t} = \lim_{\epsilon\to 0} \frac{1}{2\epsilon}\left(S_m - S_p - A_m + A_p\right) \ , \tag{7}$$

which is the expression used in the main text.

This expansion parameter ϵ, if made too small, can lead to large errors in the measurement process as well as to operations that modify the wave function very slightly, thus requiring high precision in the control instruments. At the same time, it must be small enough for the approximation to remain valid.

To implement this operator M we need a 4-dimensional ancilla that allows us to dilate the size of the Hilbert space so that we can construct the unitary matrix

$$U = \begin{pmatrix} S_m & 0 & 0 & 0 \\ 0 & -S_p & 0 & 0 \\ 0 & 0 & -A_m & 0 \\ 0 & 0 & 0 & A_p \end{pmatrix} \ . \tag{8}$$

If our system starts in state $\rho(t=0) \equiv \rho_0$, we will first have to generate the initial state $|\tilde{\rho}_0\rangle = |\rho_0 \oplus \rho_0 \oplus \rho_0 \oplus \rho_0\rangle$. Let us consider the case of a spin 1/2, where a 4-level system will be needed to encode its 4 elements of the density matrix such that $|\rho_0\rangle = \rho^0_{00}|0\rangle_s + \rho^0_{10}|1\rangle_s + \rho^0_{01}|2\rangle_s + \rho^0_{11}|3\rangle_s$, with $|i\rangle_s$ $(i = 0, \ldots 3)$ being the 4 logical levels of the physical implementation chosen. Then, for this case, the initial state $|\tilde{\rho}_0\rangle$ will be a tensor product between the state of the system and the ancilla so that

$$\begin{aligned} |\tilde{\rho}_0\rangle = &\left(\rho^0_{00}|0\rangle_s + \rho^0_{10}|1\rangle_s + \rho^0_{01}|2\rangle_s + \rho^0_{11}|3\rangle_s\right) \otimes |0\rangle_a + \left(\rho^0_{00}|0\rangle_s + \rho^0_{10}|1\rangle_s + \rho^0_{01}|2\rangle_s + \rho^0_{11}|3\rangle_s\right) \otimes |1\rangle_a + \\ &\left(\rho^0_{00}|0\rangle_s + \rho^0_{10}|1\rangle_s + \rho^0_{01}|2\rangle_s + \rho^0_{11}|3\rangle_s\right) \otimes |2\rangle_a + \left(\rho^0_{00}|0\rangle_s + \rho^0_{10}|1\rangle_s + \rho^0_{01}|2\rangle_s + \rho^0_{11}|3\rangle_s\right) \otimes |3\rangle_a \ . \end{aligned} \tag{9}$$

We see that ultimately, in order to simulate the dynamics of a two-level system using this method, we will need two 4-level qudits, one to encode the elements of the density matrix and the other as an ancilla. The final state of the system will be given by

$$|\tilde{\rho}(t)\rangle = RU|\tilde{\rho}_0\rangle = |\rho(t) \oplus \ldots\rangle \ . \tag{10}$$

Here, the operator U acts on each subspace of the ancilla, applying each of the operations S_m, $-S_p$, $-A_m$, A_p on the corresponding subspace, while the operator R is in charge of generating the appropriate superposition on the subspace corresponding to the state $|0\rangle_a$ that allows recovering the expression in (7). The remaining coefficients from the wavefunction corresponding to the other subspaces of the ancilla, $|i\rangle_a$ $(i = 1, 2, 3)$, are of no interest. Performing state tomography on the desired subspace and re-scaling by the factor 2ϵ, we recover the final coefficients: $|\rho(t)\rangle\otimes|0\rangle_a = (\rho^t_{00}|0\rangle_s + \rho^t_{10}|1\rangle_s + \rho^t_{01}|2\rangle_s + \rho^t_{11}|3\rangle_s) \otimes |0\rangle_a$. This R operation, in the present case considered of a two-level system, can be accomplished by applying a generalized Hadamard operation on the 4-level ancilla, $\tilde{H}|j\rangle_a = \frac{1}{\sqrt{4}}\sum_{k=0}^{3} \omega^{k\cdot j}|k\rangle_a$ where $\omega = e^{i2\pi/d} = e^{i\pi/2}$.

As a molecular system to implement this method we consider a complex similar to the one described in Eq. (3), only that now in addition to a spin 3/2 (which will now be the unit A corresponding to the system of interest) we also consider a spin 5/2, of which we will only use the 4 states with lowest energies (corresponding to the ancillary unit B). This choice allows us to have parameters in the spin Hamiltonian corresponding to each unit sufficiently different to be able to spectroscopically resolve each of the transitions [cf. Figure S4]. Thus, the Hamiltonian of the system will be

$$H^{(M2)}_{AMB} = \mu_B B_0 \left(g^A_z S^A_z + g^B_z S^B_z + g^M_z \left(S^M_{1z} + S^M_{2z}\right)\right) + D_A \left(S^A_z\right)^2 + D_B \left(S^B_z\right)^2 + \Delta \mathbf{S}^M_1 \cdot \mathbf{S}^M_2 + J \sum_{\alpha=A,B} \sum_{i=1,2} \mathbf{S}_\alpha \cdot \mathbf{S}^M_i \ , \tag{11}$$

with values for the parameters of $g^A_z = 1.96$, $g^B_z = 2.00$, $g^1_z = g^2_z \equiv g^M_z = 2.1$, $\Delta/2\pi = 30$ GHz, $J/2\pi = 0.2$ GHz, $D_A/2\pi = 3.0$ GHz, $D_B/2\pi = 5.2$ GHz, $B_0 = 600$ mT.

From Figure S4 it can be seen that the complexity in the control of the system increases as more resonant transitions have to be used. This is especially reflected in the number of transitions to be considered as auxiliary transitions for the controlled gates. For this method we need to decompose unitaries involving two qudits of 4 levels each. For the

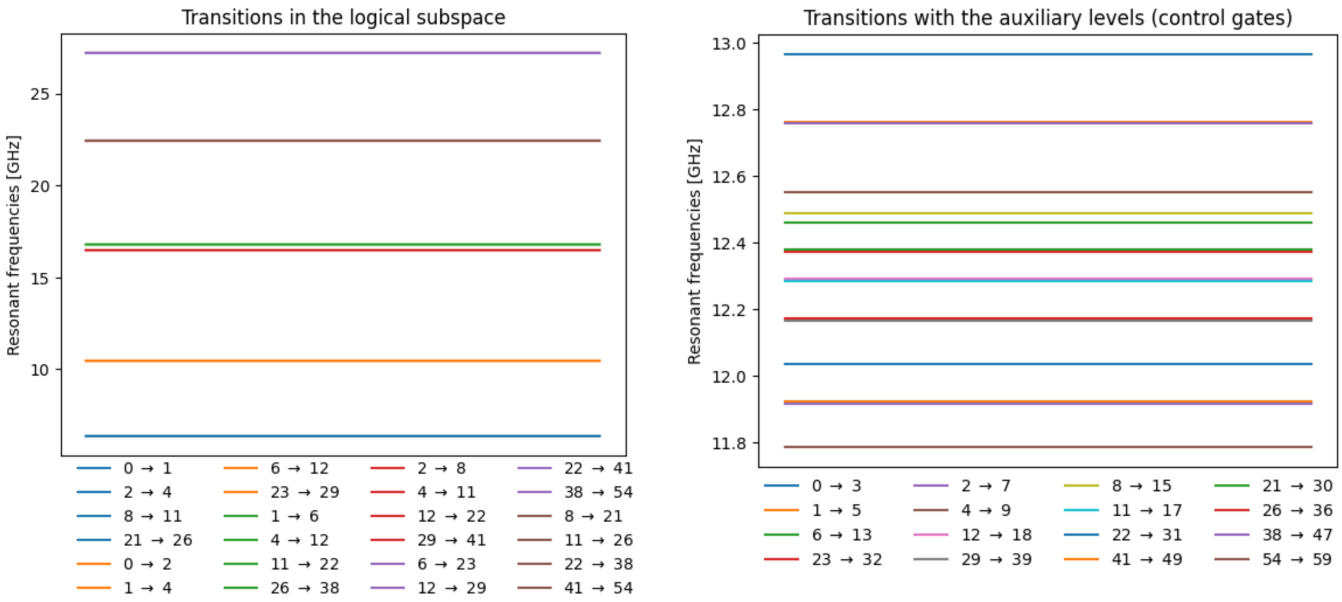

FIG. S4. Resonant frequencies for the different transitions addressed in the single qubit simulation.

implementation of each of these operations we rely on the recipe given in Ref. 9. Again, this type of implementation using the dimer as the switch of the interactions, facilitates the decomposition by containing as native gate the $C\varphi$ operation (equivalent to a $CRz(\varphi)$ gate on the working qudit controlled by a given state of the ancillary qudit). In this way we can implement the 4 different two-qudit gates $C^m[U]$: $(m = |0\rangle_a,\ U = S_m)$; $(m = |1\rangle_a,\ U = -S_p)$; $(m = |2\rangle_a,\ U = -A_m)$; $(m = |3\rangle_a,\ U = A_p)$. For each of these operations we need to implement at most 12 planar rotations and 6 Rz rotations (which in general can be implemented virtually at no practical cost) plus 6 2π-pulses on the corresponding auxiliary levels from the dimer/switch. All that remains is the implementation of the quantum adder R. This operation is a single qudit gate that we can simplify. As we have explained, we are only interested in recovering the coefficients of the wave function corresponding to the subspace of $|0\rangle$. Therefore, we only need to correctly implement the first column of the R operator, which translates into the implementation of only 3 planar rotations. This poses a total of $\mathcal{O}(99)$ operations, which is a considerable increase compared to the previous algorithm, where 10 microwave pulses in total did suffice to simulate the dynamics of Rabi oscillations damped by the DEP channel. It must be recalled that it is a particular case since a single Trotter step is enough to correctly characterize the dynamics, while this second method does not suffer from that kind of scaling. Regardless of the dynamics we want to consider (for a two-level system), the order of operations to be implemented remains the same. This difference in operations is reflected in the execution times. The results presented in Figure 2b of the main text, the complete sequence of pulses comprises about 5 μs. Note that in this case, we have not taken the measurement process into account, as we do not explicitly consider the effect of the T_2 time of the molecules on the dynamics in order to isolate the effect of the expansion parameter ε.

B. On the complexity reduction

Once again, we can observe the scaling of this algorithm compared to a platform based entirely on qubits. However, in this case, it is not as straightforward to derive an expression for the scaling of the number of operations with the number of qubits, as the unitary operations A_p, A_m, S_p, and S_p exhibit a more complex structure than the other unitaries in the previous algorithm. Therefore, we directly implement the circuits in *Qiskit* and compare them with the number of operations required on our platform, according to the analysis in Sec. II B.

For the case of $S = 1/2$, we consider the dynamics presented in the main text, which corresponds to the histogram shown in Figure 2c. For the case of $S = 3/2$, represented in Figure 1c, we consider the dynamics generated by a Hamiltonian of the form $H = D\left(S_z^2 - S(S+1)/3\right) + E\left(S_x^2 - S_y^2\right)$, with $D/2\pi = 12$ GHz and $E/2\pi = 0.3$ GHz, like in a Fe^{3+} ion in octahedral coordination[12]. The incoherent dynamics are included as the Lindblad operator $L = \sqrt{2/T_2}S_z$ with $T_2 = 1$ μs. Implementing $M = e^{\mathcal{L}t}$ as described above in Eq. (7) for $t = 300$ ns in a circuit composed of 6 linearly arranged qubits and decomposing them into native operations using Qiskit, we get 67400 ± 435 native operations after

10 runs, once again using the compiler at its highest optimization level. With our qudit-based implementation, only $O(1140)$ operations are required. For obvious reasons, we do not include an image of the resulting circuit.

IV. ON THE SCALING

To obtain the results shown in Figure 3 of the main text, two A-dimer-B complexes with the characteristic properties of Eq. (3) have been considered. Both complexes are coupled to a superconducting resonator as shown in Figure 2 of the main text, so that we exploit all possible types of interaction present in our platform. The target Ising interaction between the model spins is implemented through the interaction between the A_1 and A_2 units via the resonator; the effect of the transverse magnetic field is implemented through the coherent dynamics of each of the A_1, A_2 units through the control lines via microwave pulses; finally, the interaction between the spins and their corresponding environments is reproduced through the coupling between the A_i and B_i $(i = 1, 2)$ units mediated by the dimer.

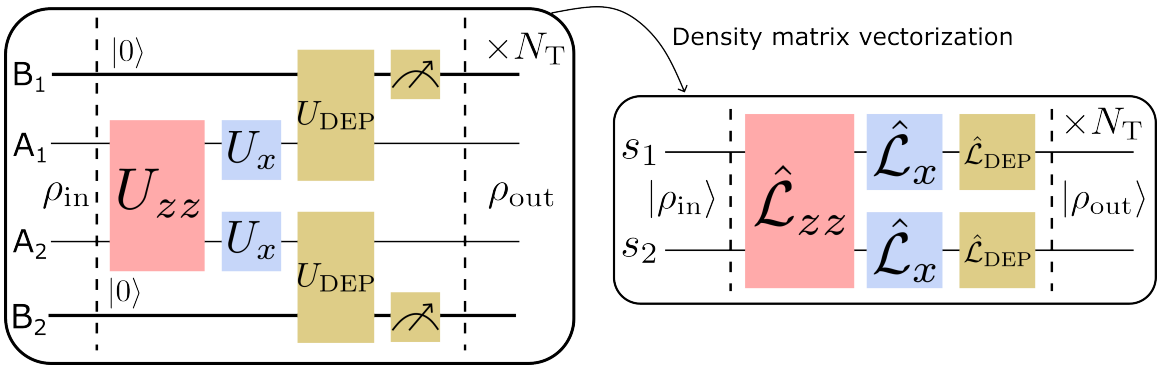

FIG. S5. Using the Choi-Jamiołkowski isomorphism, we can express the dynamics of all the operations performed on the hardware as super-operators acting on the state of the open quantum system we want to simulate. This allows us to include the non-coherent dynamics that are inevitably present in any physical implementation without simulating the entire physical system.

A. Superoperator formalism

In order to carry out the numerical simulation of the whole physical system, a different strategy has been employed to the one used in the simulations described above. Given the computational cost that would be required to simulate all the physical units at the same time, we have used the Choi-Jamiołkowski isomorphism[13,14] (also known as vectorisation of the density matrix) and the no-leakage approximation to treat the dynamics of each of the blocks of operations in the quantum circuit separately. This isomorphism allows us to obtain for each block of operations its matrix representation as a superoperator acting on the degrees of freedom of the levels involved. For example, the block corresponding to the Ising interaction between the two spins only requires the simulation of the A_1 and A_2 units interacting through the resonator, so that we can avoid the rest of the Hilbert space. The fact that we work under the no-leakage approximation ensures that the numerical simulation done in this way is identical to considering the whole physical system. Thus, the combination of all the blocks is reduced to a product of matrices containing both the dynamics induced by the coherent operations and the natural decoherence processes inherent to the physical implementation (see Figure S5).

To obtain each of the superoperators, it suffices to solve the dynamics given by Eq. (4) for each of the vectors forming the basis of the vectorised density matrix space. Note that when we introduced this equation in the previous section, it was in a different context. There the goal was for our quantum circuit to represent the dynamics given by that equation, here we use that formalism simply as a numerical tool to simulate a completely different circuit.

B. Entangling gates via superconducting resonators

As stated in the main text, the entangling gates between units A_1 and A_2 are realized by following the protocol described in Ref. 6. The main idea behind this approach is that of exploiting resonant photon absorption and emission

to implement a controlled phase gate between the qubits A_1 and A_2. The realization of such setup requires the strong coupling of molecular spins to superconducting resonators. Let us consider the coupling of the two qubits to a superconducting resonator, described by the Hamiltonian:

$$H_{qs} = \mu_B B_0(g_z^{A_1} S_z^{A_1} + g_z^{A_2} S_z^{A_2}) + \hbar\omega_0(t) a^\dagger a + 2G(S_x^{A_1} + S_x^{A_2})(a + a^\dagger) \tag{12}$$

where $a^\dagger$ and a are photon creation and annihilation operators, respectively; $\hbar\omega_0(t)$ is the tunable photon energy and G is the spin-photon coupling. Note that in H_{qs} we omitted the Hamiltonian terms involving the dimer and the B_1 and B_2 units, since the resonator frequencies are tuned only on the A_1 and A_2 energy gaps.

When performing operations on each isolated A_i-dimer-B_i system, the resonator is in its idle state, in which the photon frequency is detuned from the energy gaps of A_1 and A_2 by an energy difference $>> G$ and no photons are present in the system. This no-photon state corresponds to the computational basis of our simulations, in which resonator-qubit interaction is effectively absent and, by extent, the two qubits are uncoupled. If we now tune the resonator frequency in resonance with the energy gap of A_1, a photon gets emitted within the resonator only if the $|1\rangle_1$ state is populated. The resonator frequency is then tuned to an energy gap associated to the $|1\rangle_2$ state of the A_2 qubit and, through semi-resonant absorption and re-emission of the photon by A_2, its $|1\rangle_2$ state gains an additional phase φ. Although it is required that this energy gap should not be the A_2 qubit energy gap (in this case we might corrupt its state), the large number of states of the A_2-dimer-B_2 complex ensures that we have enough states outside of the computational basis that we can exploit to define this energy gap. As a last step, by tuning the resonator frequency to the initial A_1 qubit frequency, the photon gets re-absorbed and the $|1\rangle_1$ state is populated again.

Although this method might seem complicated, it is easy to see how it only affects the $|11\rangle$ two-qubit state and it has the effect of adding a phase to this same state, effectively implementing the entangling $C\varphi$ gate to the two-qubit system.

As a final note, let us briefly discuss the results we would expect for the simulations leading to Figure 3(d) in the main text if a molecule with $S = 1/2$ and thus total spin-photon coupling of 100 kHz were to be used. For the Q values considered in that figure, the lifetime of a photon varies between 6 and 600 μs. The time scale comprising the resonator-based entangling gate, for a total coupling of 1 MHz, corresponds to ~ 1 μs. Reducing this coupling to 100 kHz would involve an execution time of this entanglement gate of ~ 10 μs. Thus, the fidelity should now exhibit a strong dependence on Q in the $10^5 - 10^6$ range, corresponding to $6 - 60$ μs of photon lifetime respectively, and stabilizing from there. However, given the scale for the T_2 values considered, we see that the threshold from which we should recover fidelities of about 0.95 should be past $T_2 \approx 80\mu s$.

* stefano.carretta@unipr.it

[1] C. R. Harris, K. J. Millman, S. J. van der Walt, R. Gommers, P. Virtanen, D. Cournapeau, E. Wieser, J. Taylor, S. Berg, N. J. Smith, R. Kern, M. Picus, S. Hoyer, M. H. van Kerkwijk, M. Brett, A. Haldane, J. F. del Río, M. Wiebe, P. Peterson, P. Gérard-Marchant, K. Sheppard, T. Reddy, W. Weckesser, H. Abbasi, C. Gohlke, and T. E. Oliphant, Nature **585**, 357 (2020).

[2] J. Johansson, P. Nation, and F. Nori, Computer Physics Communications **184**, 1234 (2013).

[3] T. Xin, S. J. Wei, J. S. Pedernales, E. Solano, and G. L. Long, Physical Review A **96** (2017), 10.1103/PhysRevA.96.062303.

[4] P. Santini, S. Carretta, F. Troiani, and G. Amoretti, Phys. Rev. Lett. **107**, 230502 (2011).

[5] A. Castro, A. García Carrizo, S. Roca, D. Zueco, and F. Luis, Phys. Rev. Appl. **17**, 064028 (2022).

[6] A. Chiesa, S. Roca, S. Chicco, M. de Ory, A. Gómez-León, A. Gomez, D. Zueco, F. Luis, and S. Carretta, Phys. Rev. Appl. **19**, 064060 (2023).

[7] A. Palacios-Laloy, F. Nguyen, F. Mallet, P. Bertet, D. Vion, and D. Esteve, Journal of Low Temperature Physics **151**, 1034 (2008).

[8] Z. L. Wang, Y. P. Zhong, L. J. He, H. Wang, J. M. Martinis, A. N. Cleland, and Q. W. Xie, Applied Physics Letters **102**, 163503 (2013).

[9] L. E. Fischer, A. Chiesa, F. Tacchino, D. J. Egger, S. Carretta, and I. Tavernelli, PRX Quantum **4**, 030327 (2023).

[10] Qiskit contributors, "Qiskit: An open-source framework for quantum computing," (2023).

[11] A. W. Schlimgen, K. Head-Marsden, L. M. Sager, P. Narang, and D. A. Mazziotti, Physical Review Letters **127** (2021), 10.1103/PhysRevLett.127.270503.

[12] A. Abragam and B. Bleaney, *Electron paramagnetic resonance of transition ions* (OUP Oxford, 2012).

[13] M.-D. Choi, Linear Algebra and its Applications **10**, 285 (1975).

[14] A. Jamiołkowski, Reports on Mathematical Physics **3**, 275 (1972).